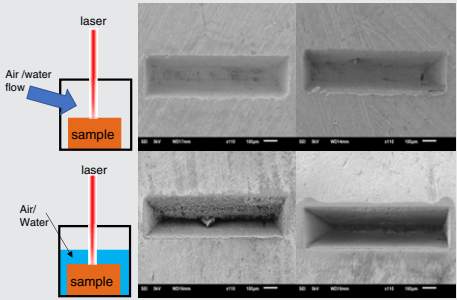Journal of
BIOPHOTONICS

FULL ARTICLE

Influence of environmental conditions in bovine bone ablation by ultrafast laser

Fahad Aljekhedab[1,2] | Wenbin Zhang[3,4,5] | Harold K. Haugen[3,6] | Gregory R. Wohl[1,7] | Munir M. El-Desouki[1] | Qiyin Fang[1,3]*

[1]School of Biomedical Engineering, McMaster University, Hamilton, Ontario, Canada

[2]National Nanotechnology Center, King Abdulaziz City for Science and Technology (KACST), Riyadh, Saudi Arabia

[3]Department of Engineering Physics, McMaster University, Hamilton, Ontario, Canada

[4]Department of Oral & Cranio-Maxillofacial Surgery, Shanghai 9th People's Hospital, Shanghai Jiao Tong University School of Medicine, Shanghai, China

[5]Shanghai Key Laboratory of Stomatology and Shanghai Research Institute of Stomatology, National Clinical Research Center of Stomatology, Shanghai, China

[6]Department of Physics and Astronomy, McMaster University, Hamilton, Ontario, Canada

[7]Department of Mechanical Engineering, McMaster University, Hamilton, Ontario, Canada

*Correspondence

Qiyin Fang, Department of Engineering Physics, McMaster University, 1280 Main Street West, Hamilton, ON L8S 4K1, Canada.
Email: qiyin.fang@mcmaster.ca

Ultrafast lasers are promising tools for surgical applications requiring precise tissue cutting. Shallow ablation depth and slow rate as well as collateral damage are common barriers limiting the use of laser in clinical applications. Localized cooling with water and/or air jet is known to reduce collateral thermal damage. We studied the influence of environmental conditions including air, compressed air flow, still water and water jet on ablation depth, ablation rate and surface morphology on bovine bone samples with an 800 nm femtosecond laser. At 15 J/cm^2, no thermal effect was observed by electron microscopy and Raman spectroscopy. The experimental results indicate that environmental conditions play a significant role in laser ablation. The deepest cavity and highest ablation rate were achieved under the compressed air flow condition, which is attributed to debris removal during the ablation process. The shallowest ablation depth and lowest ablation rates were associated with water flushing. For surface morphology, smooth surface and the absence of microcracks were observed under air flow conditions, while rougher surfaces and minor microcracks were observed under other conditions. These results suggest that ultrafast ablation of bone can be more efficient and with better surface qualities if assisted with blowing air jet.

KEYWORDS

ablation rate, bone ablation, ultrafast laser

1 | INTRODUCTION

Over the past two decades, a number of studies have looked into replacing mechanical surgical tools by lasers when cutting/drilling bone and/or cartilage [1–5]. Advantages of using laser ablation over mechanical cutting include more precise cuts, minimal mechanical stress and thermal collateral damage, the ability to work without physical contact and integration with real-time optical feedback [6, 7]. Many studies have been carried out to characterize bone ablation using infrared (IR) lasers with long pulse duration (nanoseconds to microseconds), for example, CO_2 ($\lambda = 9.6$ μm), Er:YAG ($\lambda = 2.94$ μm), Ho:YAG ($\lambda = 2.1$ μm) and Nd:YAG ($\lambda = 1.06$ μm) [3–13]. It was shown that long-pulse IR laser ablation may cause melting, carbonizing, cracking and fissuring of hard tissue [3, 14].

Fahad Aljekhedab and Wenbin Zhang contributed equally to this study.

These problems are generally attributed to the thermomechanical ablation mechanism in long pulsed ablation: when bone absorbs light energy directly, thermal expansion occurs, leading to decomposition of tissue structure [15].

In the case of ultrafast laser ablation, plasma generation within a small focal volume is the dominate ablation mechanism [16–22], where nonlinear absorption and multiphoton ionization are induced by applying high laser intensity (10^{11} W/cm^2) in the focus volume [21]. In the picosecond to femtosecond regime, the pulse duration is much shorter than thermal diffusion; hence, the ablation is confined within the focal volume. As a result, significantly lower laser fluence is required, which minimizes the thermal effect and enables highly precise (eg, submillimeter) cuts in bone [21].

Nonetheless, ultrafast lasers can remove only small amounts of hard tissue within the focal volume, which is on the order of a few micrometers per pulse [20]. Limited by current laser technology, the repetition rate of ultrafast laser ablation is also low, leading to longer time needed to produce large size structures [23]. Therefore, ultrafast lasers are generally more suitable for clinical applications where high precision control is needed, for example, pedicle screw placement in spinal surgery [23]. Nonetheless, in many hard tissue applications, the formation of deep incisions (few millimeters) into the tissue is required. Strategies to optimize ablation rate, especially the ability of achieving deep cavities are highly desired. Generally, the quantity of tissue removal increases with increasing laser fluence (J/cm^2). Thus, the increase of ablation rate (the volume of hard tissue removed by the laser per unit time, mm^3/s) can be achieved by applying high laser fluence. We have demonstrated producing large-diameter (mm diameter) holes on the cortical bone with the high fluence of laser set to 19.3 J/cm^2 (approximately six times higher than the threshold F_{th}) [16, 23]. Further increasing the fluence leads to shallower hole depth due to debris deposited on the bottom of the holes [23]. There are also concerns that high fluence may also lead to thermal damages to the crater. To minimize thermal effect and assist the ablation process, some assistive methods such as water flushing or compressed air flow (or suction) may be used [24–26]. Some studies have tried to improve ablation efficiency and minimize thermal effects using various flushing strategies with varied success. For example, the effect of water flushing on ablation efficiency is unclear. Water cooling has been reported to increase ablation efficiency in some studies, as it removes debris from the ablation area, preventing debris shielding [27, 28]. In other studies, the water absorbed a portion of the beam's energy, reducing the ablation rate [13, 17]. The effect of water on thermal damage is also unclear. Some studies show that a layer of water on the tissue surface can prevent thermal damage to adjacent tissue [29, 30], while other researchers observed tissue heating and thermal effects despite water cooling [17, 31].

In this study, we investigated the influence of ablation environmental conditions, including compressed air flow, underwater ablation and water flushing on bone tissue ablation with high fluence (~5 F_{th}). Ablation performance including ablation rate, cavity surface morphology, cut geometry, microstructure and mechanical and thermal damage induced under different ablation conditions was examined using optical, electron and Raman microscopies.

2 | EXPERIMENTAL SETUP AND METHOD

The ablation experiments were performed using an ultrafast laser machining setup shown in Figure 1A. A detailed description of the setup can be found in our previous work [16, 23, 32]. Briefly, femtosecond laser pulses (210 fs/FWHM, 200 μJ, 1 kHz, 800 nm) from an amplified Ti: Sapphire system (Tsunami-Spitfire; Spectra Physics, Santa Clara, California) is used. The collimated beam diameter was reduced to a final 1/e^2 diameter of 4.4 mm by a telescope setup. The pulse energy on the sample was controlled using the combination of a polarizer and a half-wave plate. The laser exposure time was adjusted by a computer controlled mechanical shutter (VS25S2S1; Uniblitz, Rochester, New York). The laser beam was focused onto the sample
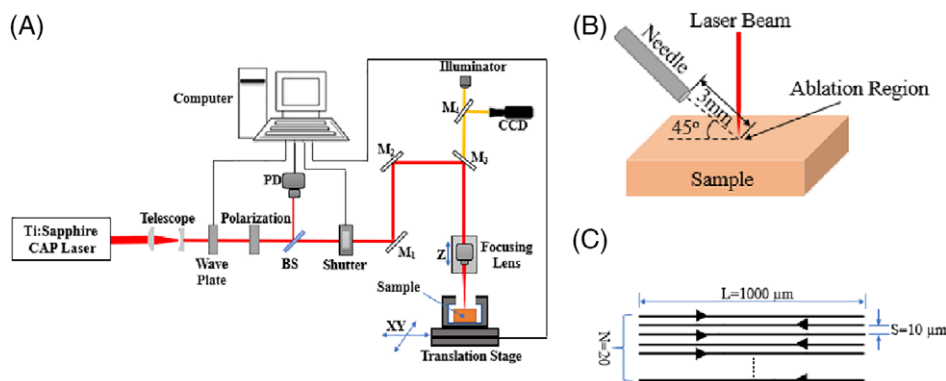

FIGURE 1   A, Schematic diagram of the ultrafast laser ablation setup. CPA, chirped-pulse amplifier; BS, beam-splitter; PD, photodiode; M_1 and M_2, high-reflection mirrors; M_3, a dichroic mirror and M_4, a beam splitter. B, Schematic setup of air flow condition. C, Schematic diagram of laser ablation path, L: scanning line length; N: number of scanning lines in one scanning pass and S: scanning line spacing

surface by a plano-convex lens (f = 12.5 cm, BK7; Thorlabs, Newton, New Jersey) to a spot size of ω_o=15.1 µm ($1/e^2$). The bone samples were placed in a glass vial sealed with paraffin wax to avoid the biological debris from leaking outside. To allow the laser beam to pass through the vial, a quartz coverslip with a thickness of 0.15 mm was used. The vial was placed on a motorized X-Y translational stage (UTM100PP.1; Newport, Irvine, California) for horizontal scanning of the sample. The focusing lens was mounted on a manual Z translation stage (MFN25PP, Newport). The ablation process was monitored using a monochrome camera and a white LED illuminator.

The experimental tissue study protocol was approved by the McMaster University Animal Research Ethics Board (AREB). Fresh bovine cortical specimens were obtained from a local butcher. All the samples were stored on ice immediately after harvesting. The connective tissue and periosteum were removed with a scalpel, and a diamond wafering saw (Buehler IsoMet, Lake Bluff, Illinois) was used to the cut the bone specimens into smaller size of $10 \times 10 \times 5$ mm. The samples were polished using a series of SiC papers (80 and 320 grit). After the laser ablation experiments, the ablated bone specimens were stored at −10°C for a few days and then examined using a reflected light microscope (Axioplane 2; Zeiss, Jena, Germany) and a scanning electron microscope (SEM 515; Philips, North Billerica, Massachusetts).

Different ablation environmental conditions were evaluated, including compressed air flow, underwater (non-flowing) and water jet flushing. The results were compared with ablation in ambient atmospheric air, that is, non-flowing. In the case of the air blowing condition, compressed air was applied on the ablation region during the ablation process. The air flow was delivered using an air pump (Electric Air Pump; Stansport, Los Angeles, CA) at 10 psi using a silicon tube and a needle with an inner diameter of 1 mm. The tip of the needle was directed under a 45° angle from vertical and 3 mm from the tissue surface, as shown in Figure 1B. For ablation with water, two different conditions were tested: (a) the sample is immersed in non-moving water with a 500 µm water layer on top of the sample surface; (b) a thin layer (500 µm thick) of water flowing on top of the sample surface during ablation process. The water flow of 1200 mL/min within the vial was produced by a micro water pump (DC micro pump, Mini26; BringSmart, Fuzhou, China). The direction of the water flow was perpendicular to the longitudinal axis of the rectangular cavity.

In all experiments, the focused beam was scanned in a raster pattern, as shown in Figure 1C, on the tissue surface (1000×220 µm^2) to produce rectangular shaped cavities. Each full rectangular raster pass consists by 20 scanning lines (length:1000 µm, line spacing:10 µm). The raster scanning speed was set at 200 µm/s with pulse energy at 55 µJ, and corresponding laser fluence at 15 J/cm^2 (~5F_{th}). The

number of scanning passes of 1 to 8 was applied to examine the effect of number of passes on ablation depth (µm) and rate (mm^3/s) under various environmental conditions. We also examined the effect of lowering focus shift during each pass. After ablation, the bone samples were cut by a diamond wafering saw parallel to the shorter axis of the rectangle cavity to expose the cross-sectional profile of the ablated region. The geometries of the cavity cross section, including depth and area, were measured two times for each crater using a reflected light microscope and analyzed using ImageJ (ver#, https://imagej.nih.gov/ij/). From the cross-section area, the volume of the ablated cavity was calculated to determine the ablation rate (mm^3/s). In addition to examine potential thermal damages, Raman analysis was carried out for the sample surface before and after the laser treatment to check for chemical composition changes. Raman spectra were obtained using a Raman spectrometer (inVia Qontor confocal Raman microscope; Renishaw, Mississauga, Canada) equipped with a He-Ne laser (model 127, Spectra Physics) operating at 633 nm. The laser beam was focused with a 50× objective lens onto the samples' surface. For each sample, five spectra were recorded with an acquisition time of 30 seconds/record. The high background levels recorded in all spectra resulted from the samples' rough surfaces. As a result, the band wave numbers were determined by fitting the experimental data with polynomial curves using Fityk (v.1.3.1, fityk.nieto.pl).

3 | RESULTS AND DISCUSSION

In the above experiments, we systematically examined the effect of ablation environmental conditions on the depth of the ablated crater, ablation rate, crater surface morphology and potential thermal side effects on the crater surface.

3.1 | Ablation depth

The crater depth (the distance from the surface to the deepest point in the bottom of the crater) as a function of the number of scanning passes at various environmental conditions is shown in Figure 2. For all four conditions, increasing of the number of scanning passes produced deeper cavities. In the entire range of scanning passes under examination, the maximum ablation depth was achieved with compressed air flow; while the shallow cavity was observed under the condition with non-flowing air. In the cases where still or flowing water were used, the cavity depths were shallowest. With refocusing objective lens (100 µm) after each scan, the increase in ablation depth was observed only under the flowing air conditions as shown in Figure 2. There was negligible effect of refocusing on the depth when non-flowing air or water conditions used (not shown in Figure 2).

Under the condition of non-flowing air, the ablation depth increased rapidly over the first three scanning passes
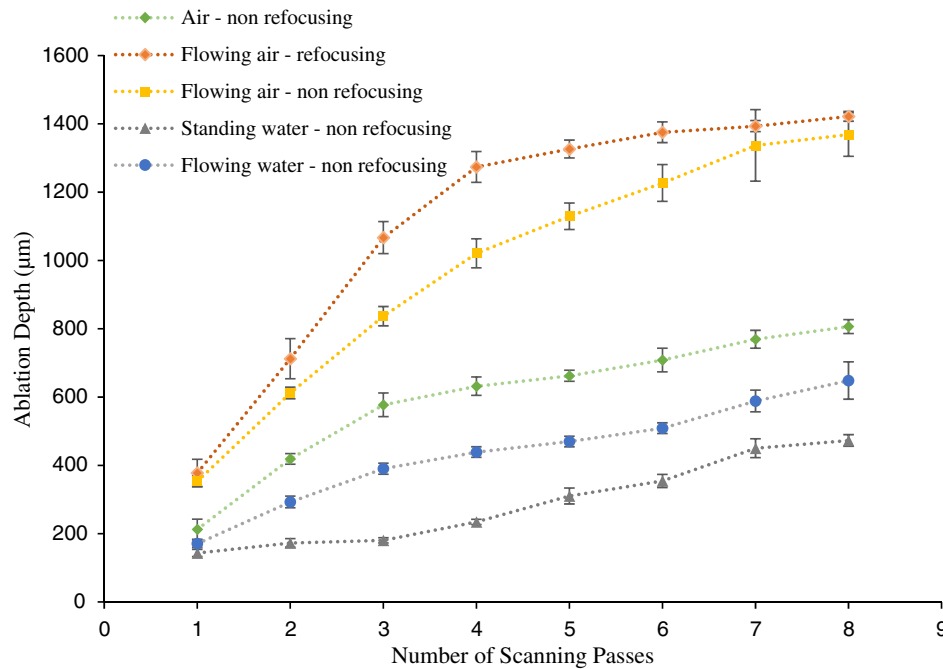
FIGURE 2 Ablation depth of the cavity as a function of the number of scanning passes for bovine bone under different experimental conditions using 15 J/cm² fluence, 200 μm/s scanning velocity and 1 kHz repetition rate. Error bars indicate SD

up to about 580 μm (Figure 2). After the first three passes, the amount of ablation with each pass decreased. This result is likely due to the influence of ablation debris, that is, the amount of ablation debris accumulates in the crater [33, 34]. Under the compressed air flow condition, the ablation depth of the cavities was much greater with each scanning pass compared with the non-flowing air condition. The compressed air flow condition also had a decreased rate of ablation after three passes, at about 820 μm, when the focus depth was not changed between successive scans. In this case, the change in the amount of ablation can be explained in relation to the Rayleigh length (where the maximum energy density is achieved) which was calculated to be 818 μm for the focusing lens used. With a deeper cut depth, some debris at the bottom of the ablated crater cannot be moved by air flow and could affect the ablation process and depth for both cases (non-refocusing and refocusing).

In the cases of ablation under non-flowing air, it was found that bone ablation was always accompanied by the debris deposited inside the irradiated region. During ablation, debris in the path of laser light can absorb and scatter the incident beam [27, 33]. Consequently, the debris shielding attenuates the pulse energy, leading to decrease in ablation depths of the craters compared to those of air flow. In contrast, the presence of flowing air during the ablation process removes the debris, leading to clean processes and deeper ablation depth than ablation near the threshold. In contrast, a study by Le et al [25] found that compressed air flow had little effect on ablation rate, likely because their work dealt with less debris. We found that air flow improves ablation depth by removing debris. Moreover, the present study used a low scanning speed (0.2 mm/s) and short pulse

duration (210 fs), two factors that create lots of debris in the ablation area. Le et al [25] used a higher scanning speed (5 mm/s) and longer pulse duration (560 fs), producing relatively little debris.

During femtosecond laser ablation, multiphoton ionization initiates optical breakdown and plasma formation [35]. The plasma-mediated ablation process is accompanied by bubble formation and subsequent material removal at the focal spot [36]. In the presence of water, the incoming laser beam interaction with water may cause non-linear phenomena such as filamentation, supercontinuum generation and optical breakdown of water, which forms a plasma shielding effect reducing the amount of energy reaching the tissue [36, 37]. In addition, another source of energy shielding is generated in the water during the formation of cavitation bubbles, scattering the incident laser beam [38]. It has been reported that energy shielding can play an important role at relatively high laser fluence [35, 38]. It has been reported that that the energy loss is estimated to be 30% to 70% of the total incident beam energy [37–40]. This explains why the smallest cut depths were obtained with still and flowing water conditions compared to air and flowing air (Figure 2). In the still water case, significant ablation debris suspended in the water layer was observed above the treatment region after the ablation process, and this debris can interfere with the incident laser beam, which further reduces the pulse energy reaching the targeted area. Consequently, shallower craters were produced using still water compared with flowing water (Figure 2) [41]. Le et al [25] did not observe any significant difference between wet and dry conditions. Their methods are different from those used in the present study, where a layer (~500 μm thick) of standing or flowing water was
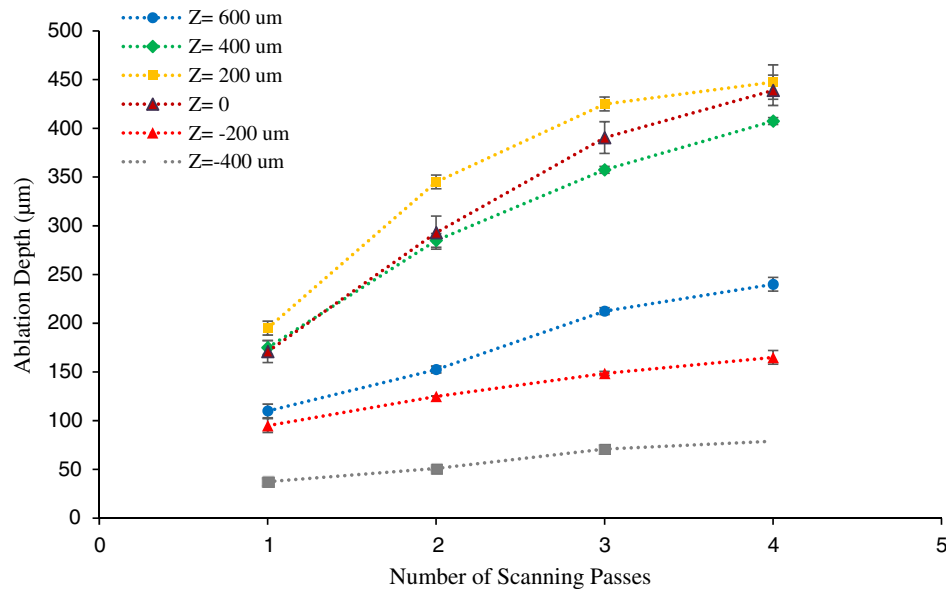
FIGURE 3 Ablation depth as a function of the number of scanning passes at different axial position of the focus position with respect to the bone surface under flowing water condition

applied to the sample surface during ablation. The water attenuated the beam before it reached its target, reducing ablation depth. In the study of Le et al [25], the water layer was diverted from the ablation area by an air jet, allowing the beam to pass without obstruction.

When ablating near the optical breakdown fluence, plasma shielding may play a role in the focal volume. At fluence much higher than the threshold (e.g. $5 \times F_{th}$ in the present study), a larger plasma area is generated above the focus, thus a significant amount of the beam energy can be absorbed by the plasma formed before the beam waist [34, 39, 42]. To reduce the plasma shielding effect and thus increase the cut depth of the crater in water ablation, the target position with respect to the objective focal plane must be considered. Additional flowing water irradiation experiments were carried out to study the effect of the position of the target surface with respect to the focal plane of the objective. The position of the focusing lens was shifted over the Z-axis, and the laser fluence at the focal point was kept constant at 15 J/cm². The positive values of Z (the focus was below the sample surface) and negative values (the focus was the above the bone surface) were investigated with different number of passes as shown in Figure 3. The results show that the deeper cavities were achieved when the target is before the focal plane by 200 μm. The same behavior was observed by Sylvestre et al [40], who reported that the highest amount of ablated material (weak plasma shielding) was found when the target was positioned slightly above the focal plane. Tulea et al [42] also reported that the plasma shielding effect due to an optical breakdown in water was avoided when the target was before the focal plane. Nonetheless, even though the deeper cut depth was obtained when target is posited above focal plane in water experiments, the

air and flowing air conditions provide deepest cut depth at the same number of passes.

3.2 | Ablation rate

A key limitation of ultrafast lasers in orthopedic applications is the slow material removal rates (mm³/s) [5]. In the present work, the enhancement of ablation rate under various experimental conditions was investigated. To measure the ablation rate, cavities with cross-section area of 1000×220 (μm²) were produced in bone sample. The depth of the cavity under different conditions is a measure of the ablation rate. First, the ablation depth increases as after each additional scan passes (shown in Figure 3). For all ablation conditions, the ablation rate decreased as the number of scanning passes increases (shown in Figure 4), that is, as the laser ablates deeper, it becomes less efficient in removing materials. This is attributed to that the increase in scanning passes produced a debris layer that resulted in the reduction of laser intensity [43, 44].

As shown in Figure 4, the highest ablation rate was achieved using flowing air-assisted ablation compared to the other three conditions. With air flow, the ablation rate is about 1.6 times higher than without blowing air. This is attributed to ablation debris being removed away from the treatment area during the ablation process by the flowing air. In the air-only case, a thick debris layer was observed in the processing area after ablation regardless of the number of scanning passes. The debris blocks the laser energy from reaching the targeted ablation volume by absorbing and scattering the incoming pulses.

In the flowing water case, even though debris effect was visibly absent, a lower ablation rate was found than those of air or flowing air. Ablation accompanies with flowing water
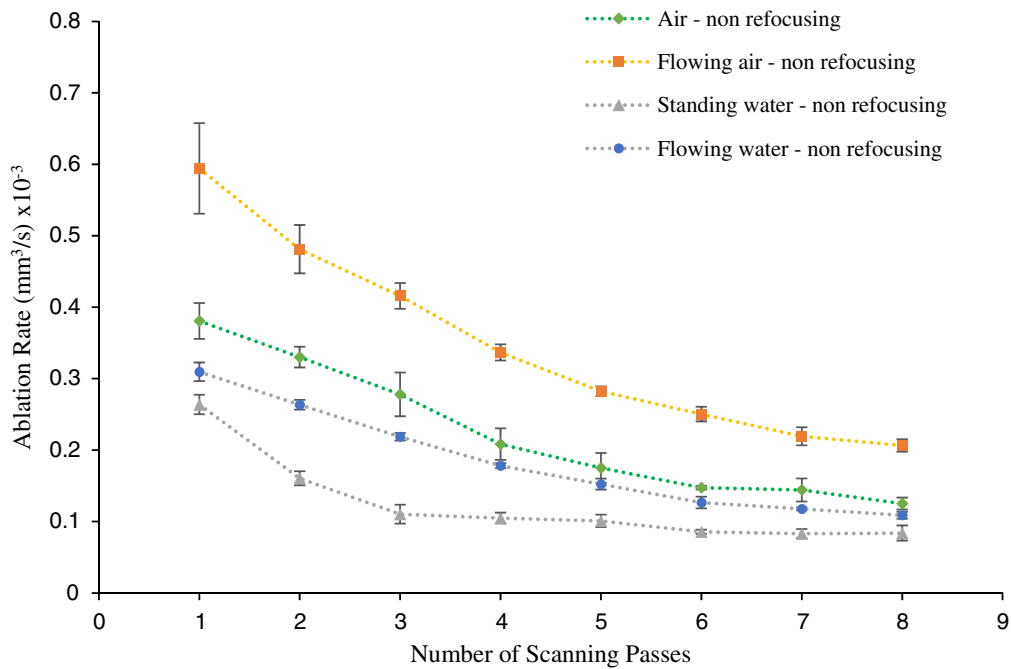
FIGURE 4 Ablation rate as a function of the number of scanning passes for bovine bone under air, flowing air, still water and flowing water using 15 J/cm^2 fluence, 210 fs pulse duration, 200 um/s scanning velocity and 1 kHz repetition rate. The error bars represent the SD of the data

removed ~20% and 50% less material (by volume) per second than those of the air and air flow processes, respectively. The slowest ablation rate was observed when a still water layer was used. The decrease in the ablation rate under water (flowing or not) can be explained by the influence of plasma shielding during ablation process [37, 38, 42, 45].

3.3 | Surface morphology

The surface morphology characterization was performed using scanning electron microscope (SEM). The ablation pattern produced cavities with depths of 632 (air), 1021 (air flow), 234 (still water) and 439 μm (water flow). Top-view SEM images of the ablation craters for the four conditions are depicted in Figure 5. Even though high fluence (~5F_{th}) was applied, the overall view shows well-defined geometry and smooth cavity rims for all four environments. This can be explained by the fact that the amount of ablated tissue per pulse (μm/pulse) is small, it increases two or three times (from ~1 to 2 or 3 μm/pulse) when the fluence increases from ablation threshold (F_{th}) to high fluence for femtosecond lasers [17, 20, 24]. However, it is reported that at high ablation rates (eg, 300, 80 and 14 um/pulse for Er lasers, Ho:

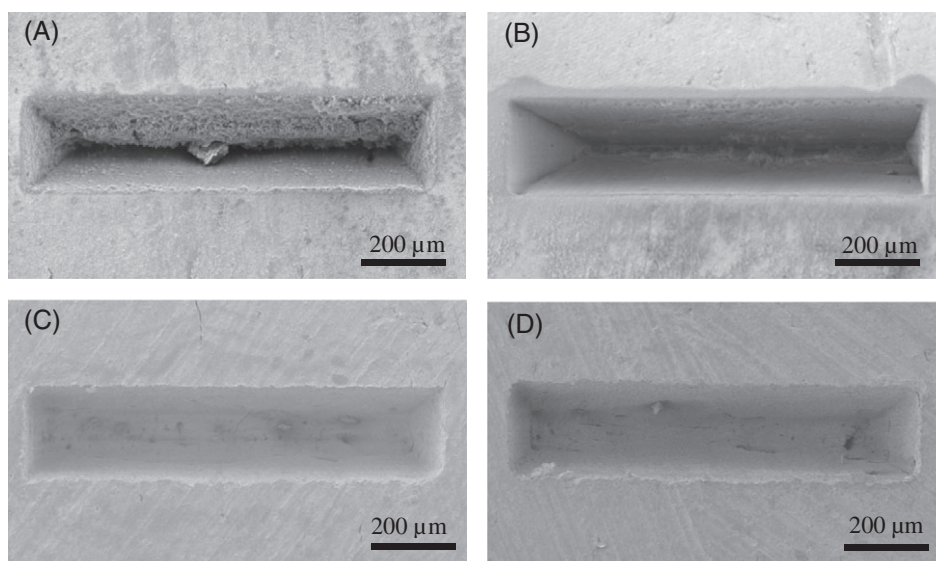**FIGURE 5** Scanning electron microscope (SEM) images of craters in bovine bone performed by repeating a 1000 × 220 (μm^2) rectangular scanning pattern four times under; A, air (cavity cleaned by air flow before image taken for characterization purpose), B, compressed air flow, C, still water, D, flowing water conditions, with laser fluence 15 J/cm^2 and scanning speed 200 μm/s
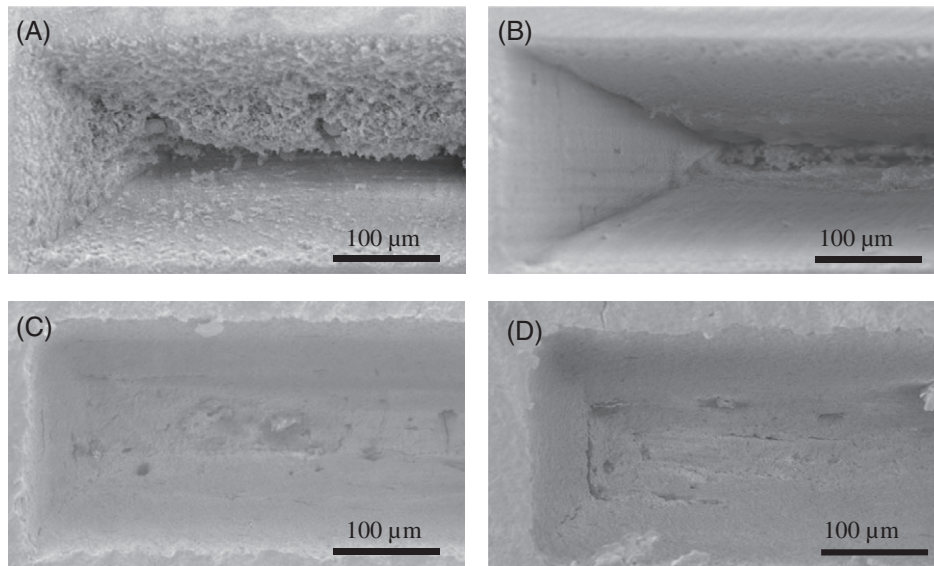
FIGURE 6 A higher magnification scanning electron microscope (SEM) view of the left side craters in bovine bone ablated by repeating the scanning pattern four times at 15 J/cm^2 fluence and 200 μm/s traverse speed under; A, air, B, compressed air flow, C, still water, D, water flow conditions

YSGG and Nd:YAG, respectively), the crater edges become irregular and rough [4, 8, 46]. Compared with the cavity edges produced by only air or both water conditions (Figure 5A,C,D), cavities created by the air flow process showed smoother surfaces (Figure 5B). The smoothness of air flow ablation could result from the relatively clean process (ie, free of debris). In water experiments (Figure 5C,D), the specific mechanism causing rough crater edges is unknown. These may be due to the optical breakdown of water and a resulting pressure impact from bubble dynamics or from molten tissue and ablation debris that are not fully flushed away from the cavity edges during ablation [47, 48].

In Figure 5, the SEM images of the craters ablated using high fluence (~5F$_{th}$) showed the absence of mechanical surfaces damage such as cracks at the crater edges for all four experimental conditions. This indicates that using a femtosecond laser at high fluence and low scanning speed (200 μm/s) and repetition rate (1 kHz) is safe for the surrounding bone tissue under the four studied environments. The preservation of the surrounding tissue is highly desirable for various surgical applications such as preparing the bone for implants [48]. A few studies reported the formation of small microcracks around treated areas using femtosecond lasers when high pulse repetition rates and low scanning velocity were applied [44]. Large cracks in the range of hundreds of microns were observed with short and long pulsed laser ablation (nanosecond to millisecond pulse widths) [8, 24].

In the non-flowing air case, a large amount of ablation debris was observed around the treatment area and at the bottom of the cavity. It was found that the debris amount increased with the number of scanning passes (more material removal). The debris accumulation layer did not adhere to the top surface of tissue and can be removed by air flow before the SEM imaging for characterization purpose [26].

As shown in Figure 5A, the debris layer attaching to the side wall cavity cannot be removed after ablation [44]. With air flow, the cavity with a small aspect ratio (depth/width ≈ 3) did not show signs of debris material on its surface or its inner walls. However, at high aspect ratio (more than three), some ablation debris accumulated at the bottom of the cavity (Figure 5B). This is due to (shown in Figure 1B) the air flow at a 45° angle is not able to completely remove the ablation debris from the cavity with a high aspect ratio. A higher efficiency of removing debris during the ablation process can be achieved by setting the air flow angle to be more perpendicular to the tissue surface and using a higher air inflation. Experimentally, we found that using air flow to clean the treatment area during the ablation process produced cleaner cavities compared to those cleaned after ablation. In both water conditions, the craters were relatively clean without any debris in the treatment area as shown in Figure 5C,D.

To investigate the shape of the side walls and the bottom of the cavities, a high magnification SEM view of the cavities side wall (left side of the cavity shown in Figure 5) is shown in Figure 6. For all four environments, the morphology of the cavity walls appears to be uniform without surface ripples. A few studies reported that femtosecond laser ablation could induce ripples on inner wall surfaces [45, 49]. As shown in Figure 6, the smoothest inner wall surface was produced with air flow (Figure 6B), which can be a result of the clean ablation process induced by air flow-assisted ablation. In both underwater cases, the inner wall surface of the cavity was rougher (Figure 6C,D). A possible explanation might be that the cavity acts as a trap to plasma expansion and confines the hydrodynamic motion of cavitation bubbles in water, which generates high pressure impacts on the cavity walls [34, 45, 50].

For all investigated conditions, the floor of the craters has a well-defined geometry with sharp edges and corners.
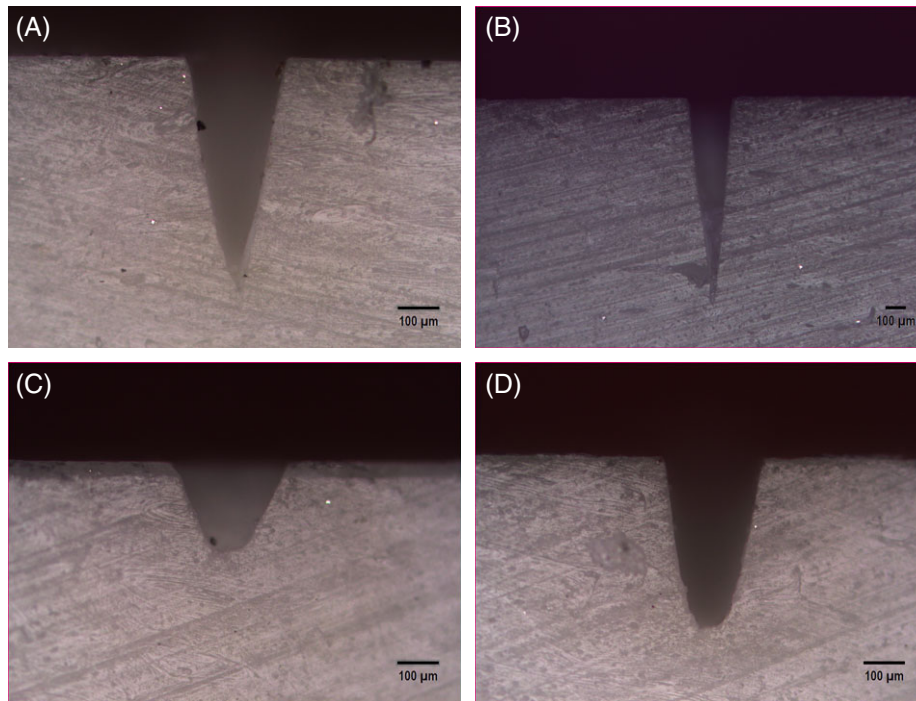
FIGURE 7 Cross section optical microscope images of craters on the bone ablated by repeating rectangular scanning pattern four times over the sample surface with 15 J/cm^2 fluence and 200 μm/s scanning speed under; A, air, B, compressed air flow, C, still water, D, water flow conditions

In air and air flow cases, a peak and valley pattern has emerged on the cavity bottom (not shown). In contrast, the floor of the crater of the water-assisted ablation was relatively flat with the presence of microcracks (Figure 6C,B), which were resulted from the high pressure induced in the confined volume of water in the cavity [51].

After ablation, the bone samples were cut perpendicular to the ablation crater using a precision diamond wafering saw and examined under an optical microscope to investigate the cavity profile. In an ideal case, the cavity cross-sectional profile should look rectangular, with the same width from the top of the cavity to the bottom. In all experimental conditions, the cavities were showing a crater profile, which is wider near the top and narrower near the crater bottom. Wider cavity near the top was produced in both underwater experiments compared with those of in air and air flow. The same result was reported by Ren and Charee [50, 51]. For all environments, it has been seen that the crater profile has a "V" shape, when aspect ratio (depth/width) is greater than two as shown in Figure 7A,B. In contrast, the cavity profile becomes a "U" shape when aspect ratio is two or less as depicted in Figure 7C,D. Several factors may contribute to such crater profiles. First, when the crater goes deeper, the laser beam energy is attenuated due to the large focus angle [5]. Second, the ablated materials cannot escape from the deep crater fast enough and thus they absorb and scatter laser beam [27]. Third, during large-scale tissue removal, the beam could scatter from the sidewall to the structure center [52].

3.4 | Thermal side effects

One of the main advantages of femtosecond laser ablation is the absence of undesired thermal side effects. The beam energy deposited by the femtosecond laser pulses does not have enough time to move into the bulk of the sample because the thermal relaxation time for biological tissue is in the order of nanoseconds to microseconds. Thus, for ultrafast ablation using focused light, the absorbed thermal energy and associated damage are confined within the focal volume. The thermal energy diffusing beyond the ablation focus volume is generally negligible [22, 25, 53, 54]. Nonetheless, a few studies have demonstrated thermal effects during femtosecond laser ablation, including carbonization and melting [45, 46, 55]. Nicolodelli et al [55], using a fluence of 5 J/cm^2, observed signs of melting in several small regions when the effective number of pulses per spot was increased to 1000. Cangueiro and Vilar [46] also observed thermal effects under dry conditions at 2 J/cm^2. Thermal effects occur when heat accumulates more quickly than it can dissipate. High laser fluence, low scanning speeds and high repetition rates are more likely to cause thermal effects because these factors allow the laser to quickly deposit heat to concentrated areas of tissue [46]. The present study used a femtosecond laser with a high fluence (15 J/cm^2), a low scanning speed (200 μm/s) and a repetition rate of 1 kHz. It is therefore appropriate for this study to explore the thermal effects of femtosecond lasers.

In the present work, the thermal side effects of femtosecond laser ablation under different conditions were examined
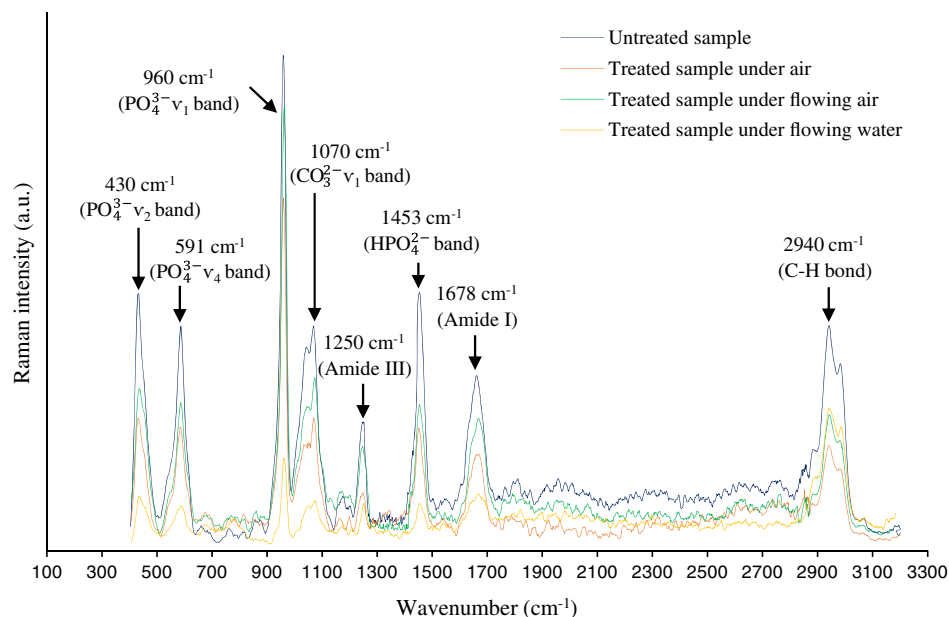
FIGURE 8 Raman spectra of bovine bone sample before and after treatment under different conditions showing the major bands corresponding the organic and inorganic bone components

using a confocal Raman microscope. Raman spectra were obtained over the wavenumber range of 400 to 3200 cm^{-1} from the untreated sample (black curve) and ablated sample as shown in Figure 8. For comparative purposes, the spectrum of an untreated sample was measured. The signal levels of the treated and untreated samples were various, likely because of differences in surface roughness. Rode et al and Cangueiro et al [3, 56] observed similar behavior. All the Raman bands recorded in the spectra of examined samples were assigned to bone compositions. No new phases such as amorphous carbon peak at 1580 and 1350 cm^{-1} were observed due to the laser ablation under different conditions which indicate that no carbonization occurred [7]. Despite the laser's high fluence and low scanning speed, we observed no thermal damage in any experimental conditions, in stark contrast to previous studies [46, 55]. This is likely because previous studies had more overlapping pulses (the effective number of pulses per spot), increasing heat accumulation. In this study, there were only 94 pulses per spot, compared with 1000 and 6283 pulses per spot in Nicolodelli et al [55] and Cangueiro's studies [56], respectively. These results indicate that a high fluence, when mitigated by low overlapping pulses, is less likely to cause thermal damage. For all Raman spectra of samples, the clear peaks around 430, 591 and 960 cm^{-1} were observed correspond to the phosphate inorganic component. The spectra present the ν_1 vibration band of CO_3^{2-} at 1070 cm^{-1} and the bending vibration band of the HPO_4^{2-} ion at 1453 cm^{-1} correspond to carbonate and phosphate mineral components, respectively. The two peaks at 1250 and 1678 cm^{-1} provide evidence of existing the organic collagen protein, the amide I and III. The carbon-hydrogen (C-H) bond was observed at 2940 cm^{-1} corresponded to organic component of bone.

4 | CONCLUSION

We studied laser ablation of bovine bone using a femtosecond laser under various environmental conditions at high fluence (~5F_{th}). The ablation depth, rate, surface morphology and thermal effects were investigated to provide an overview of the influence of different environments on the ablation process. It was found that experimental conditions have a considerable influence on the investigated factors. The deeper cavities and faster ablation rates were obtained under air flow compared with those of only air or water. The effect of debris on the ablation depth and rate was observed in air case. With water, shallowest depths and slowest rate were measured due to the loss of beam energy due to plasma shielding. For all environments, precision cavities in bone were obtained and no signs of microcracks or thermal effects were observed. Our results suggest that compressed air flow is an effective assistive method to achieve deeper ablation, smoother crater surfaces and with negligible thermal damage even at high fluence levels.

ORCID

Qiyin Fang https://orcid.org/0000-0003-2786-9884

REFERENCES

[1] R. Marjoribanks, C. Dille, J. Schoenly, L. McKinney, A. Mordovanakis, P. Kaifosh, P. Forrester, Z. Qian, A. Covarrubias, Y. Feng, L. Lilge, *Photon. Lasers Med.* **2012**, *1*, 155.

[2] B. Mirdan, D. Batani, L. Volpe, A. Villa, M. Bussoli, R. Jafer, M. Veltcheva, P. Procacci, V. Conte, *J. Laser Micro, Nanoeng.* **2013**, *8*, 192.

[3] A. Rode, E. Gamaly, B. Davies, B. Taylor, M. Graessel, J. Dawes, A. Chan, R. Lowe, P. Hannaford, *Aust. Dent. J.* **2003**, *48*, 233.

[4] M. Strassl, V. Wieger, D. Brodoceanu, F. Beer, A. Moritz, E. Wintner, *J. Laser Micro, Nanoeng.* **2008**, *3*, 30.

[5] J. Neev, L. Silva, M. Feit, M. Perry, A. Rubenchik, B. Stuart, *IEEE J. Sel. Top. Quant. Electron.* **1996**, *2*, 790.

[6] R. Menezes, C. Harvey, M. Gerbi, Z. Smith, D. Smith, J. Ivaldi, A. Phillips, J. Chan, S. Wachsmann-Hogiu, *J. Biophotonics* **2017**, *10*, 1292.

[7] R. Gill, Z. Smith, C. Lee, S. Wachsmann-Hogiu, *J. Biophotonics* **2016**, *9*, 171.

[8] X. Zhang, Z. Zhan, H. Liu, H. Zhao, S. Xie, Q. Ye, *J. Biomed. Opt.* **2012**, *17*, 038003.

[9] J. Youn, P. Sweet, G. Peavy, *Lasers Surg. Med.* **2007**, *39*, 332.

[10] B. Ivanov, A. Hakimian, G. Peavy, R. Haglund, *Appl. Surf. Sci.* **2003**, *208*, 77.

[11] N. Fried, D. Fried, *Lasers Surg. Med.* **2001**, *28*, 335.

[12] M. Buchelt, H. Kutschera, T. Katterschafka, H. Kiss, S. Lang, R. Beer, U. Losert, *Lasers Surg. Med.* **1994**, *15*, 373.

[13] H. Kang, J. Oh, A. Welch, *Phys. Med. Biol.* **2008**, *53*, 3381.

[14] B. Kim, M. Feit, A. Rubenchik, E. Joslin, P. Celliers, J. Eichler, S. Da, *J. Biomed. Opt.* **2001**, *6*, 332.

[15] M. Ivanenko, G. Eyrich, E. Bruder, P. Hering, *Lasers Life Sci.* **2000**, *9*, 171.

[16] B. Emigh, R. An, E. Hus, T. Crawford, H. Haugen, G. Wohl, J. Hayward, Q. Fang, *J. Biomed. Opt.* **2012**, *17*, 028001.

[17] M. Silva, M. Wehner, C. Eduardo, F. Lampert, R. Poprawe, M. Hermans, M. Oliveira, *Lasers Med. Sci.* **2013**, *28*, 171.

[18] M. Kamata, T. Imahoko, K. Ozono, M. Obara, *Appl. Phys. A* **2004**, *79*, 1679.

[19] J. Kraft, K. Vestentoft, B. Christensen, H. Lovschall, P. Balling, *Appl. Surf. Sci.* **2008**, *254*, 1895.

[20] B. Girard, D. Yu, M. Armstrong, B. Wilson, C. Clokie, R. Miller, *Lasers Surg. Med.* **2007**, *39*, 273.

[21] A. Vogel, J. Noack, G. Huttman, G. Paltauf, *Appl. Phys. B* **2005**, *81*, 1015.

[22] R. Lizarelli, M. Costa, E. Filho, F. Nunes, V. Bagnato, *Laser Phys. Lett.* **2008**, *5*, 63.

[23] R. An, G. Khadar, E. Wilk, B. Emigh, H. Haugen, G. Wohl, B. Dunlop, M. Anvari, J. Hayward, Q. Fang, *J. Biomed. Opt.* **2013**, *18*, 070504.

[24] A. Rode, E. Gamaly, B. Davies, B. Taylor, J. Dawes, A. Chan, R. Lowe, P. Hannaford, *J. Appl. Phys.* **2002**, *92*, 2153.

[25] Q. Le, R. Vilar, C. Bertrand, *Lasers Med. Sci.* **2017**, *32*, 1943.

[26] Q. Le, C. Bertrand, R. Vilar, *J. Biomed. Opt.* **2016**, *21*, 125007.

[27] M. Ivanenko, P. Hering, *Appl. Phys. B* **1998**, *67*, 395.

[28] H. Kang, H. Lee, S. Chen, A. Welch, *IEEE J. Quantum Elect.* **2006**, *42*, 633.

[29] L. Kuscer, J. Diaci, *J. Biomed. Opt.* **2013**, *18*, 108002.

[30] J. Hoke, E. Burkes, E. Gomes, M. Wolbarsht, *Laser Appl.* **1990**, *2*, 61.

[31] D. Fried, N. Ashouri, T. Breunig, R. Shori, *Lasers Surg. Med.* **2002**, *31*, 186.

[32] A. Borowiec, H. Haugen, *Appl. Phys. A* **2004**, *79*, 521.

[33] H. Kang, I. Rizoiu, A. Welch, *Phys. Med. Biol.* **2007**, *52*, 7243.

[34] A. Vogel, V. Venugopalan, *Chem. Rev.* **2003**, *103*, 577.

[35] Q. Fang, X. Hu, *IEEE J. Quantum Electron.* **2004**, *40*, 69.

[36] L. Mortensen, C. Alt, R. Turcotte, M. Masek, T. Liu, D. Côté, C. Xu, G. Intini, C. Lin, *Biomed. Opt. Express* **2015**, *6*, 32.

[37] A. Vogel, J. Noack, K. Nahen, D. Theisen, S. Busch, U. Parlitz, D. Hammer, G. Noojin, B. Rockwell, R. Birngruber, *Appl. Phys. B* **1999**, *68*, 271.

[38] G. Daminelli, J. Kruoger, W. Kautek, *Thin Solid Films* **2004**, *467*, 334.

[39] W. Liu, O. Kosareva, I. golubtsov, A. Iwasaki, A. Becker, V. Kandidov, S. Chin, *Appl. Phys. B* **2003**, *76*, 215.

[40] J. Sylvestre, A. Kabashin, E. Sacher, M. Meunier, *Appl. Phys. A* **2005**, *80*, 753.

[41] V. Tangwarodomnukun, J. Wang, P. Mathew, *Key Eng. Mat.* **2010**, *443*, 693.

[42] C. Tulea, J. Caron, H. Wahab, N. Gehlich, M. Hoefer, D. Esser, B. Jungbluth, A. Lenenbach, R. Noll, *Proc. SPIE.* **2013**, *8565*, 85656.

[43] H. Chen, H. Li, Y. Sun, Y. Wang, P. Lü, *Sci. Rep.* **2016**, *6*, 20950.

[44] J. Kaakkunen, M. Silvennoinen, K. Paivasaari, P. Vahimaa, *Phys. Proc.* **2011**, *12*, 89.

[45] H. Liu, F. Chen, X. Wang, Q. Yang, H. Bian, J. Si, X. Hou, *Thin Solid Films* **2010**, *518*, 5188.

[46] L. Cangueiro, R. Vilar, *Appl. Surf. Sci.* **2013**, *283*, 1012.

[47] A. Tamura, T. Sakka, K. Fukami, Y. Ogata, *Appl. Phys. A* **2013**, *112*, 209.

[48] N. Krstulovic, S. Shannon, R. Stefanuik, C. Fanara, *Int. J. Adv. Manuf. Technol.* **2013**, *69*, 1765.

[49] L. Ji, L. Li, H. Devlin, Z. Liu, J. Jiao, D. Whitehead, *Lasers Med. Sci.* **2012**, *27*, 197.

[50] J. Ren, M. Kelly, L. Hesselink, *Opt. Lett.* **2005**, *30*, 1740.

[51] W. Charee, V. Tangwarodomnukun, C. Dumkum, *Int. J. Adv. Manuf. Technol.* **2015**, *78*, 19.

[52] B. Emigh, Master Thesis, McMaster University (Hamilton, Canada), **2011.**

[53] A. Daskalova, S. Bashir, W. Husinsky, *Appl. Surf. Sci.* **2010**, *257*, 1119.

[54] A. Vorobyev, C. Guo, *Appl. Phys. Lett.* **2005**, *86*, 011916.

[55] G. Nicolodelli, R. Lizarelli, V. Bagnato, *J. Biomed. Opt.* **2012**, *17*, 048001.

[56] L. Cangueiro, R. Vilar, A. Rego, V. Muralha, *J. Biomed. Opt.* **2012**, *17*, 125005.